Gelation via Ion Exchange in Discotic Suspensions

Ya-Wen Chang,[1] Andres F. Mejia,[1] Zhengdong Cheng,[1,2,3,*] Xiaojun Di,[4] and Gregory B. McKenna[4]

[1]*Artie McFerrin Department of Chemical Engineering, Texas A&M University, College Station, Texas 77843, USA*
[2]*Material Science and Engineering Program, Texas A&M University, College Station, Texas 77843, USA*
[3]*Professional Program in Biotechnology, Texas A&M University, College Station, Texas 77843, USA*
[4]*Department of Chemical Engineering, Whitacre College of Engineering, Texas Tech University, Lubbock, Texas 79409, USA*

(Received 10 March 2011; revised manuscript received 30 April 2012; published 15 June 2012)

The phase behavior of charged disk suspensions displays a strong dependence on ionic strengths, as the interplay between excluded volume and electrostatic interactions determines the formation of glasses, gels, and liquid crystal states. The various ions in natural soil or brine, however, could present additional effects, especially considering that most platelet structures bear a momentous ion-exchange capacity. Here we observed how ion exchange modulates and controls the interaction between individual disks and leads to unconventional phase transitions from isotropic gel to nematic gel and finally to nematic liquid crystals.

DOI: 10.1103/PhysRevLett.108.247802 PACS numbers: 64.70.M−, 82.70.Dd, 82.70.Gg, 83.80.Hj

Colloidal dispersions of charged anisotropic particles exhibit an intriguingly wide range of rheological properties and rich liquid crystal phase behaviors. The ability of nonspherical particles to undergo a spontaneous disorder-to-order, i.e., isotropic-to-nematic (*I-N*), liquid crystal transition at high particle concentrations was first demonstrated theoretically by Onsager [1] as a purely entropy-driven process due to particle-shape anisotropy. Stable liquid crystal phases formed by platelike particles were later confirmed by computer simulations [2,3]. In addition, disordered states, such as gels or glasses, are particularly prominent in charged systems [4–6]. They were thought always to intervene with the observation of stable nematic phases, with the most notable example of nonreproducible *I-N* separation in hectorite suspensions observed by Langmuir [7]. However, research in the past decade has revealed the existence of nematic phases for selected natural and synthetic clays [8–10], whose *I-N* transition occurred at a concentration lower than the sol-gel transition point that is strongly dependent on the ionic strength of the solvent. To date, there seems to be little work showing the ionic strength controlled phase diagrams of charged, discotic suspensions that display both a gel phase and stable liquid crystal phases. The detailed study here will elucidate gelation of discotic suspensions that readily form liquid crystal phases under normal conditions. These gels are vastly different from structures of nematic liquid crystal embedded in a secondary matrix, the so-called nematic gels [11,12]. The ability to precisely describe gel structure and its formation in such systems is of vital importance to their technological applications such as use as rheology modifiers and fillers in composite materials.

An aqueous suspension of high-aspect-ratio, charge-stabilized zirconium phosphate (ZrP) platelets prepared by exfoliation was recently shown to exhibit stable nematic alignment at low-volume fractions [13]. As with clay, the ion-exchange property of α-ZrP has long been exploited in applications such as nuclear waste treatments and kidney dialysis; hence, its structure and physiochemical properties are well characterized. In this Letter, we present the phase diagram of these equal-thickness platelets as a function of salt and particle concentrations. Different phases were distinguished and characterized with polarized imaging, rheology, and light scattering. We find that a strong specific attraction induced by ion exchange leads to gelation of the suspension; conversely, with insufficient ion exchange, repulsive interactions remain dominant, drawing the system back to a liquid crystal state.

We synthesized α-zirconium phosphate pristine (layered) crystals by using a hydrothermal procedure [14] and exfoliated them with tetrabutyl ammonium hydroxide (TBAOH) at a molar ratio of TBAOH:α-ZrP = 1:1 to obtain stable colloidal suspensions of monolayered ZrP in deionized water. Excess TBAOH was removed by centrifugation at 4000 g for 2 h, and the platelets were resuspended in deionized water. Completely exfoliated platelets have an identical thickness of 2.68 nm [15,16] and an average diameter D, determined by dynamic light scattering. Several batches ($B1$–$B4$) of particles were prepared in this study, and minimal variations in size and polydispersity were present ($D = 1325$ nm, polydispersity $\sigma = 32\%$ for the $B1$ batch; $D = 1093$ nm, $\sigma = 32\%$ for the $B2$ batch; $D = 1485$ nm, $\sigma = 36\%$ for the $B3$ batch; $D = 1431$ nm, $\sigma = 34\%$ for the $B4$ batch). The concentration of the stock suspension was determined gravimetrically by drying a fixed amount of the suspension at 60 °C. Stock suspensions were diluted with deionized water or salt solutions to obtain the desired particle concentrations and ionic strengths.

We investigated the influence of ionic strength on the *I-N* transition of ZrP suspensions. Tetrabutylammonium chloride (TBACl), a salt with an identical cation to the exfoliating agent, was chosen first to avoid complication of the system, and the samples were monitored through cross-polarizers. Figure 1(a) shows cross-polarized

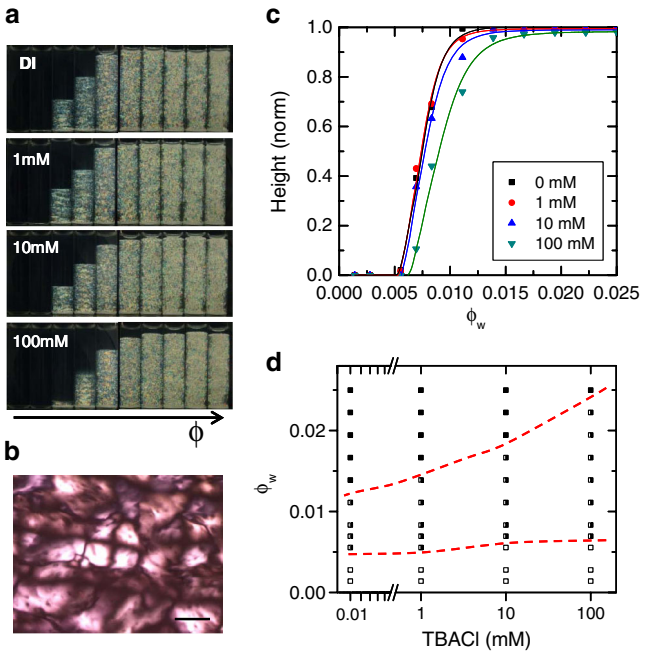

FIG. 1 (color online). Influence of TBA salt concentration on the ZrP platelet phase diagram. (a) Polarized light photograph of ZrP platelet suspensions at particle concentrations of 0.28, 0.56, 0.69, 0.83, 1.11, 1.39, 1.67, 1.94, 2.22, 2.50 wt. % in TBACl solutions. (b) Schlieren texture of a nematic suspension. Scale bar: 150 μm. (c) Nematic height as a function of salt and particle concentrations. (d) Summarized phase diagram. Phase states include isotropic liquid (open rectangle), biphasic (half-filled rectangle), and nematic (filled rectangle). The dashed curve outlines the biphase region.

photographs of monolayer platelets at ten concentrations, increasing from left to right, suspended in 0- to 100-millimolar ionic strength solutions. For a fixed ionic strength, very dilute particle suspensions showed strong flow birefringence under cross-polarizers. At increased particle concentrations (in the *I-N* coexistence region), the suspensions became permanently birefringent and exhibited nematic defects in polarizing microscopy [Fig. 1(b)]. Over the course of 48 h, complete phase separation occurred for these two-phase coexistent samples into an upper isotropic and a lower nematic phase, separated by a visibly sharp interface. Figure 1(c) gives a snapshot of the progressive increase of nematic volume fraction in the samples with the overall platelet weight fraction for varying ionic strengths. At fixed particle concentrations (weight fraction ϕ_w) within the biphase region, the fraction of nematic appears increasingly reduced with the increase of ionic strengths, a phenomenon anticipated as a result of the decrease in repulsion as is observed in clays [17]. The boundaries of the biphasic gap can be extrapolated by a nonlinear fit (due to wide polydispersity [13]) in Fig. 1(c) to the height-concentration curve. Figure 1(d) summarizes the TBACl-dependent phase diagram: The lower boundary $\phi_{w,I}$ was essentially unchanged up to an ionic strength of 10 mM; the full nematic phase $\phi_{w,N}$ was obtained at $0.011 \leq \phi_{w,N} \leq 0.014$ for ionic strengths below 1 mM, $\phi_{w,N} \sim 0.017$ for 10 mM, and $\phi_{w,N} > 0.022$ for 100 mM (exact position not determined). This increase in $\phi_{w,N}$ with ionic strength is in qualitative agreement with the screening of electrostatic repulsion with ions. In the study of crystallization in suspensions of charged colloidal spheres, fluid-crystal coexistence increases with ionic strength to a maximum at the hard sphere limit [18].

Theoretical calculations on infinitely thin hard platelets [2] have shown that *I-N* phase transitions occur between densities $\rho_{\mathrm{iso}}D^3 = 3.7$ and $\rho_{\mathrm{nem}}D^3 = 4.0$ for monodispersed suspensions, where ρ is the number density of the transitions and D the platelet diameter. Since our system exhibits high polydispersity, it is reasonable to compare experimental with the theoretical values for polydispersed samples ($\sigma \sim 32\%$), whose densities are found to be $\rho_{\mathrm{iso}}D^3 = 3.5$ and $\rho_{\mathrm{nem}}D^3 = 5.6$ (according to Ref. [2]). Following van der Beek and Lekkerkerker [9], the relation between core volume fraction ϕ and the number density for platelets of diameter D, thickness t, and polydispersity σ is

$$\rho\langle D\rangle^3 = 8/9\sqrt{3}(\langle D\rangle/\langle t\rangle)(1 + 3\sigma^2)/(1 + \sigma^2)\phi. \quad (1)$$

Taking into account the geometrical factor after exfoliation (layer thickness increased by threefold due to the attachment of TBA^+), we convert weight percents into disk ϕ values by an approximate density value of $\sim$1.8 g/cm^3. Equation (1) yields dimensionless densities of $\rho_{\mathrm{iso}}D^3 = 2.1$ and $\rho_{\mathrm{nem}}D^3 = 5.2$ for our suspensions at zero ionic strength. The results are comparable to theoretical values; discrepancies might be due to platelet geometry or surface charges.

In addition to liquid crystal phases, gelled phases occurred when a common salt—sodium chloride (NaCl)—was used to adjust the suspension ionic strength instead of TBACl. Figure 2 presents the optical photographs of a series of suspensions in 0 (as a reference for the salt-free phase diagram), 10, and 20 mM NaCl, providing preliminary evidence of gelled states, in which samples were able to retain air bubbles due to finite yield stresses. Gelled samples at a platelet concentration below $\phi_w = 0.011$ for both 10 and 20 mM ionic strength appeared isotropic; for the 20 mM series, those whose concentrations were in the range $0.011 \leq \phi_w \leq 0.021$, on the other hand, displayed strong birefringent textures. For the 10 mM ionic strength series, reentrance of the stable liquid crystalline phase was found at concentrations above 0.011. Biphasic samples (with clear phase separation) were observed at $0.011 \leq \phi_w \leq 0.021$, within which the proportion of lower nematic phase increases with the concentration of particles. Full nematic fluid was obtained at $\phi_w \approx 0.028$. Similarly, for the 20 mM series, the suspensions appeared fluid again at $\phi_w > 0.021$ (Fig. S2 [19]). The nature of these higher particle and salt concentration samples is less obvious, as they appear diffusive in bulk (path length $\sim$9 mm) due to

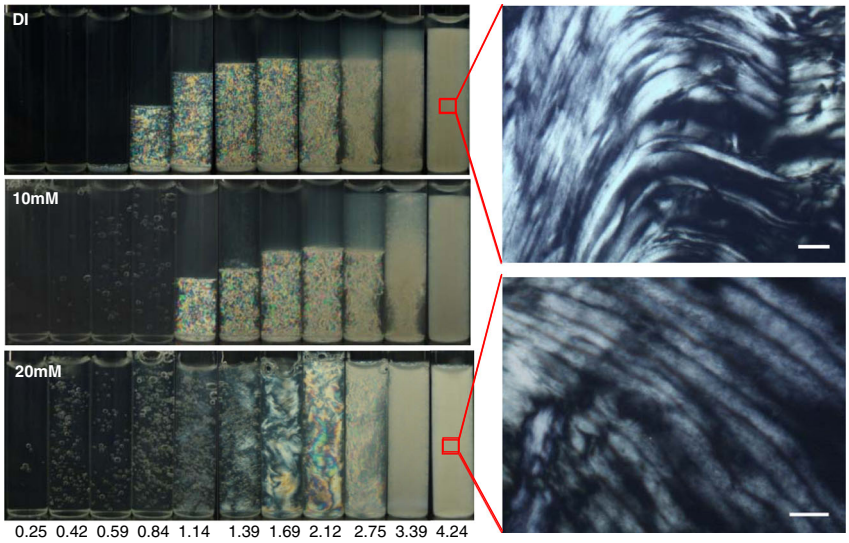

FIG. 2 (color online). Polarized images of ZrP suspensions ($B3$ batch) in 0, 10, and 20 mM NaCl salt solutions. Left: Photographs of bulk samples at increasing ϕ (left to right, labeled concentration in wt. %). Right: Microscopy images of high concentration liquid crystal phases. Scale bar: 50 μm.

the high refractive index of zirconium phosphate. As flocculated samples could also appear birefringent as a consequence of scattering from aggregated (anisotropic) clusters, it is important to demonstrate sample homogeneity via bright-field imaging. The absence of optical contrast viewed in regular light (Fig. S3 [19]) verifies its homogenous nature, and the suspension can be recognized as a liquid crystalline phase by the pronounced optical texture under polarized microscopy imaging, similar to that in zero ionic strength (Fig. 2, right).

Formation of gel structures was further verified and characterized with rheology and light-scattering measurements. Small-amplitude oscillatory shear experiments were carried out by using a Parr-Physica MCR-300 rheometer with parallel plate geometry (25 mm plate diameter, gap of 0.5 mm) at 25 °C. The samples were presheared at 500 s^{-1} and relaxed for 8 min. The elastic and viscous moduli G' and G'' were measured at a strain amplitude of $\gamma = 0.02$ with angular frequencies from 0.01 to 100 s^{-1} (Fig. S2 [19]). Figure 3(a) shows the elastic modulus G' (value at 1 s^{-1}) as a function of ϕ_w at 20 mM NaCl for selected gel samples from the $B3$ batch, where the reduced positive dependency of G' with particle concentrations is demonstrated. The result differs dramatically from previous studies on anisotropic colloidal gels [20–22], whose storage modulus followed a power law dependence on reduced particle volume fraction $(\phi - \phi_0)^n$ at fixed ionic strength ($n = 2.3$–2.5 for clay suspensions; ϕ_0 is the critical ϕ above which gel appears). At this salt concentration, the gel characteristic eventually disappeared at $\phi_w > 0.021$.

Multispeckle diffusive wave spectroscopy in backscattering geometry [23,24] was used to identify arrested or nonarrested structures. The samples were illuminated with a 633 nm laser, and the backscattered light was collected onto a CCD camera at 90 frames/s. The ensemble average autocorrelation function is obtained from

$$g_2(t) = \langle I_i(0) I_i(t) \rangle / \{ \langle I_i(0) \rangle \langle I_i(t) \rangle \}, \quad (2)$$

where I_i refers to the intensity of backscattering light at the ith pixel, which is a function of time. The correlation function g_2 quantitatively describes the similarity between two images at different times. In general, relaxation time (or decorrelation time) is defined as the time required for g_2 to decay to half its value at time zero. Slower decay of g_2 or longer relaxation time indicates slower particle motions, a sign for restricted motion for frozen systems such as glassy materials and colloidal gels. Figure 3(b) shows g_2 versus time for six samples ($B4$ batch) at aging time around 2 h, with concentrations spanning through broader phase states than that included in Fig. 3(a)—isotropic gel (samples 1 and 2), nematic gel (samples 3 and 4), and

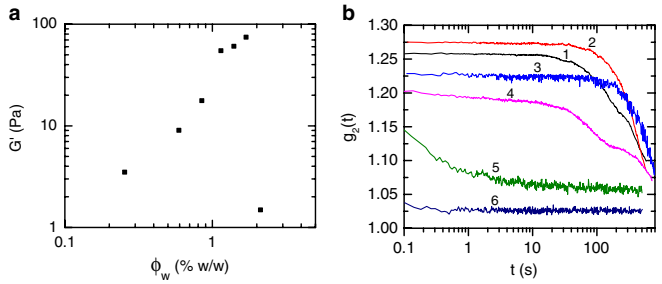

FIG. 3 (color online). (a) Evolution of the elastic modulus as a function of platelet ($B3$ batch) concentration at an ionic strength of 20 mM. (b) Autocorrelation functions of varying ZrP ($B4$ batch) concentrations (from 1 to 6, 0.36, 0.71, 1.07, 2.13, 2.84, 4.26%) at a fixed NaCl concentration and aging time ($\sim$ 2 h).

fluidic liquid crystal phase (samples 5 and 6). Correlation functions of samples 1–4 showed a significant long relaxation time, typical of arrested states. Dramatic relaxation-time reduction was apparent for higher concentration samples (5 and 6), confirming an ungelling transition when ϕ_w increased from 0.021 to 0.028 ($B4$ batch, 20 mM NaCl). Additionally, an aging phenomenon (the evolution of the correlation function with time) was observed for gel-state samples while being absent for liquid crystal samples (data not shown), providing corroborating evidence for the transition.

The liquid crystal and sol-gel phase behaviors in NaCl solutions were evaluated by using the above-described methodologies (see [19]) and mapped onto a two-dimensional phase diagram (Fig. 4). At salt concentrations below 10 mM, the offset of phase boundaries is qualitatively consistent with the TBACl case. In contrast to the TBACl system, where the dispersion appears stable up to 100 mM ionic strength, gelation occurred for NaCl concentrations larger than 10 mM. The location of the gel region determined by rheology and light-scattering data infers unprecedented gel-to-liquid crystal transitions upon increasing the particle concentration at fixed ionic strengths. Although arrested states are encountered frequently in charged platelet systems, the phase behavior of the NaCl-ZrP system is different from the gelling behavior observed for most natural or synthetic clays, where the percolated networks expand throughout the entire sample with particle concentrations above the sol-gel transition [8,17,21,22,25]. The unique phase evolution pathway suggests an intrinsically different mechanism for the gelling behavior of ZrP platelets in the presence of NaCl.

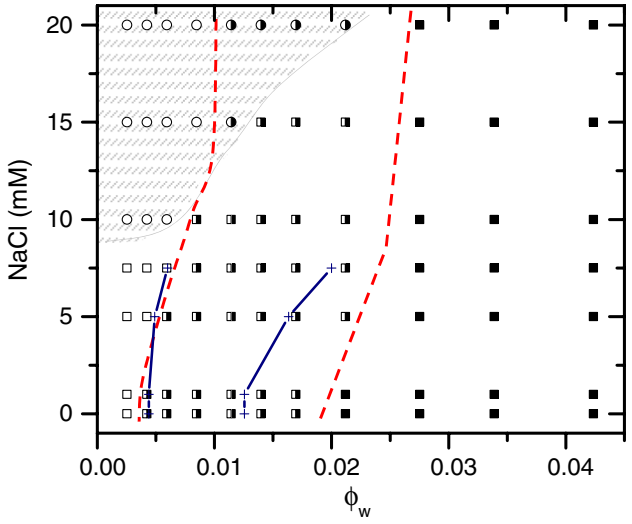

FIG. 4 (color online). State diagram as a function of platelet and NaCl concentration. Phase states include isotropic liquid (open rectangle), isotropic gels (open circle), birefringent gels (half-filled circle), biphasic (half-filled rectangle), and nematic (filled rectangle) liquid crystals. Shaded areas represent the gelled phase, and the biphase region is outlined for both polydispersed ($B3$ batch, dashed lines) and more monodispersed ($B2$ batch, crosses linked with solid lines) samples.

To rationalize this unusual phase behavior, we take a closer look at the structure of the monolayer platelets, the origin of the gel phase, and how the surface charges and interparticle interactions are modified with the addition of NaCl. Since the exfoliated monolayer platelet $Zr(HPO_4)(TBAPO_4)$ consists of half-exchanged α-ZrP, with a layer of TBA^+ packing on the platelet surface and an underlying residual hydroxyl group in between each TBA^+, ion exchange could proceed in the presence of NaCl as Na^+ displaces the available protons or the loosely bound TBA^+ on the surfaces (Fig. S5 [19]). Release of the dissociated H^+ into the suspension from the proton displacement process can be detected, as shown in Fig. 5—a significant, continuous drop of suspension pH with the addition of NaCl until a plateau value of ~3.3 was reached. The suspension enters an arrested state at the approximate equal molar ratio of NaCl to ZrP, where the pH value drops below 5.5. Direct acidification using HCl also yields a similar sol-gel transition (data not shown), indicating that $p\mathrm{H} = 5.5$ is the critical point where strong attraction arises, presumably in the face-edge direction due to opposite charges at the rims and faces of the platelets [19].

From the aspect of ion exchange, the interpretation of the phase behavior as a function of NaCl concentration and packing fraction can now be refined as follows. At low ionic strength (0 to 7.5 mM), where the effect of surface charge alteration is minimal due to limited ion exchange [molar ratio of $Zr(HPO_4)(TBAPO_4)/\mathrm{NaCl} \gg 1$], the influence of ionic strength can be considered to be an electrostatic screening one, similar to TBACl cases. At higher ionic strengths and low particle concentrations [$\mathrm{NaCl} > 7.5$ mM, $Zr(HPO_4)(TBAPO_4)/\mathrm{NaCl} \leq 1$], ion exchange between Na^+ ions and surface protons reduces

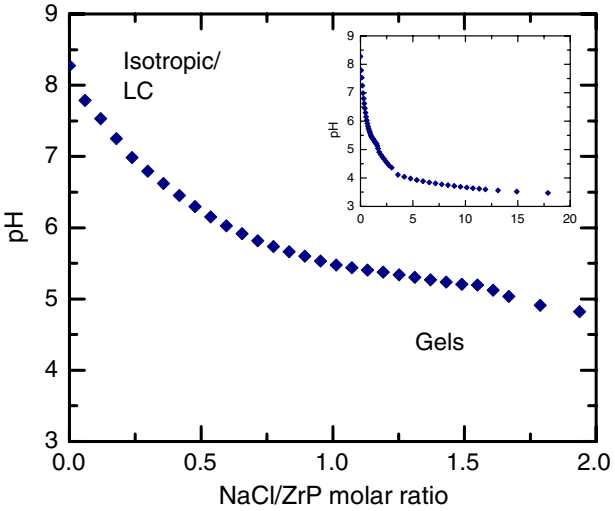

FIG. 5 (color online). Suspension pH evolution with added NaCl concentration. Inset: pH at broader NaCl/ZrP ratios.

the suspension pH below 5.5, and a transition from repulsive to attractive interactions takes place, causing gelled phases to appear. The decrement in suspension pH (i.e., concentration of protons released), controlled by the degree of ion exchange, is roughly proportional to NaCl concentration and inversely proportional to particle concentration according to the chemical balance of the exchange reaction. Therefore, for constant ionic strength, the degree of ion exchange decreases with increasing particle volume fraction (less pH reduction), which leads to an overall weaker attraction at higher particle concentrations. This explains the gel-to-liquid crystal transition upon increasing platelet fractions that is consistent with the general trend of jamming phase transitions (as a change in interaction potentials) [26].

In summary, we have studied the ionic strength dependent phase diagram of ZrP monolayer platelets and validated the use of ion exchange to induce anisotropic interactions among individual platelets. Liquid crystal states and arrested states were identified and confirmed via polarized imaging, rheology, and diffusive wave scattering techniques. Unlike regular clay suspension cases, fluidization occurs at increasing particle concentrations for (NaCl) ionic strength above ≈ 8 mM, where low-volume fraction gels started to form. The gelling transitions were shown to depend strongly on suspension pH (a consequence of ion exchange at different NaCl/ZrP ratios), a parameter expected to influence charge interactions. The results offer a novel observation of the gelling behavior of charged discotic suspensions as ion-exchange (pH) - modulated interactions come into play. Our work opens up new routes to the formation of discotic colloidal gels, and the comparison with other charged platelet systems should contribute to a better understanding of the role of ion exchange that is fundamental to charged discotic materials.

We thank Y. Martinez-Raton, E. Velasco, and A. Clearfield for discussions useful to the content of this Letter. Acknowledgment is made to V. Ugaz for the use of the rheometer. This work is supported by NSF DMR-1006870 at TAMU and NSF CBET-1133279 at Texas Tech University.

*To whom all correspondence should be addressed.
zcheng@tamu.edu

[1] L. Onsager, Ann. N.Y. Acad. Sci. **51**, 627 (1949).
[2] M. A. Bates and D. Frenkel, J. Chem. Phys. **110**, 6553 (1999).
[3] J. A. C. Veerman and D. Frenkel, Phys. Rev. A **45**, 5632 (1992).
[4] D. van der Beek and H. N. W. Lekkerkerker, Europhys. Lett. **61**, 702 (2003).
[5] J. C. P. Gabriel, C. Sanchez, and P. Davidson, J. Phys. Chem. **100**, 11 139 (1996).
[6] A. Mourchid, A. Delville, J. Lambard, E. LeColier, and P. Levitz, Langmuir **11**, 1942 (1995).
[7] I. Langmuir, J. Chem. Phys. **6**, 873 (1938).
[8] L. J. Michot, I. Bihannic, S. Maddi, S. S. Funari, C. Baravian, P. Levitz, and P. Davidson, Proc. Natl. Acad. Sci. U.S.A. **103**, 16 101 (2006).
[9] D. van der Beek and H. N. W. Lekkerkerker, Langmuir **20**, 8582 (2004).
[10] H. Hemmen, N. I. Ringdal, E. N. De Azevedo, M. Engelsberg, E. L. Hansen, Y. Meheust, J. O. Fossum, and K. D. Knudsen, Langmuir **25**, 12 507 (2009).
[11] T. C. Lubensky, R. Mukhopadhyay, L. Radzihovsky, and X. Xing, Phys. Rev. E **66**, 011702 (2002).
[12] D. Lacoste, A. W. C. Lau, and T. C. Lubensky, Eur. Phys. J. E **8**, 403 (2002).
[13] D. Z. Sun, H.-J. Sue, Z. Cheng, Y. Martínez-Ratón, and E. Velasco, Phys. Rev. E **80**, 041704 (2009).
[14] L. Y. Sun, W. J. Boo, H.-J. Sue, and A. Clearfield, New J. Chem. **31**, 39 (2007).
[15] H.-N. Kim, S. W. Keller, T. E. Mallouk, J. Schmitt, and G. Decher, Chem. Mater. **9**, 1414 (1997).
[16] L. Sun, W. J. Boo, D. Sun, A. Clearfield, and H.-J. Sue, Chem. Mater. **19**, 1749 (2007).
[17] N. I. Ringdal, D. M. Fonseca, E. L. Hansen, H. Hemmen, and J. O. Fossum, Phys. Rev. E **81**, 041702 (2010).
[18] W. B. Russel, D. A. Saville, and W. R. Schowalter, in *Colloidal Dispersions* (Cambridge University Press, Cambridge, England, 1999), p. 347.
[19] See Supplemental Material at http://link.aps.org/supplemental/10.1103/PhysRevLett.108.247802 for the details of the phase diagram, the proof of sample homogeneity, and the discussion on a plausible gelling mechanism.
[20] L. J. Michot, C. Baravian, I. Bihannic, S. Maddi, C. Moyne, J. F. L. Duval, P. Levitz, and P. Davidson, Langmuir **25**, 127 (2009).
[21] A. Mourchid, E. Lécolier, H. Van Damme, and P. Levitz, Langmuir **14**, 4718 (1998).
[22] L. J. Michot, I. Bihannic, K. Porsch, S. Maddi, C. Baravian, J. Mougel, and P. Levitz, Langmuir **20**, 10 829 (2004).
[23] V. Viasnoff, F. O. Lequeux, and D. J. Pine, Rev. Sci. Instrum. **73**, 2336 (2002).
[24] X. J. Di, K. Z. Win, G. B. McKenna, T. Narita, F. Lequeux, S. R. Pullela, and Z. Cheng, Phys. Rev. Lett. **106**, 095701 (2011).
[25] M. C. D. Mourad, D. V. Byelov, A. V. Petukhov, D. A. Matthijs de Winter, A. J. Verkleij, and H. N. W. Lekkerkerker, J. Phys. Chem. B **113**, 11 604 (2009).
[26] V. Trappe, V. Prasad, L. Cipelletti, P. N. Segre, and D. A. Weitz, Nature (London) **411**, 772 (2001).